Direct Model Predictive Control of a Single-Phase Grid-Connected Siwakoti-H Inverter

Mirza Abdul Waris Begh*, Eyke Liegmann†, Petros Karamanakos*, and Ralph Kennel†
*Faculty of Information Technology and Communication Sciences, Tampere University, 33101 Tampere, Finland
Email: *mirza.begh@tuni.fi, p.karamanakos@ieee.org
†Chair of Electrical Drive Systems and Power Electronics, Technical University of Munich, 80333 Munich, Germany
Email: †eyke.liegmann@tum.de, ralph.kennel@tum.de

***Abstract*—The Siwakoti-H flying-capacitor inverter (sFCI) is a recent member of the family of transformerless inverters. Due to its minimal design, it presents a favorable alternative to conventional transformerless topologies. One of the major challenges in the control of the sFCI is to maintain the flying capacitor voltage within prescribed limits. To address this issue, a direct model predictive control (MPC) scheme is proposed for a single phase grid-connected sFCI. A discrete-time switched nonlinear model of the converter is derived, which captures the dynamics of the flying capacitor and the LCL filter. The nonlinear model enables the accurate prediction of the system behavior over the whole operating range. The proposed MPC strategy is tasked to work in two different modes, i.e., grid-disconnected mode and grid-connected mode, with specific control objectives. The presented results demonstrate the flying capacitor voltage control in grid-disconnected mode, and also illustrate the steady-state and dynamic performance of the controller in grid-connected mode.**

I. Introduction

Power electronic converters are enabling technologies for conversion and control of electric power in grid-connected systems, accomplished by virtue of a pattern of switching operations applied to the semiconductor switches. In renewable energy systems like wind turbine and photovoltaic (PV) systems, the ability to attain high efficiency has been the main driver in the past decade. One of the measures to reduce losses in the system is to employ a converter topology with less switching elements. Additionally in PV systems, there has been an increasing trend to use transformerless converters [1]. Among the recently proposed topologies, the Siwakoti-H inverter [2], [3] is a common-ground-type transformerless inverter which consists of only four switches and works on the principle of a flying capacitor. The uniqueness of this topology is that the positive and the negative voltage bus requirement can be fulfilled by using a single input capacitor, thereby reducing the input voltage requirement compared to the conventional neutral point clamped (NPC) converter [4].

Previously, the control of the grid-connected sFCI was investigated using a state-feedback controller [4], [5]. The controller gives good steady-state performance for the sFCI, but it suffers from uneven deviation near the zero crossing, see [5, Fig. 7]. This behavior is due to the abrupt change in the source from input capacitor C_{in} to the flying capacitor C_{FC}. In order to mitigate this issue and achieve faster dynamic response, an indirect model predictive control (MPC) scheme was proposed for a three-phase grid-connected sFCI in [6].

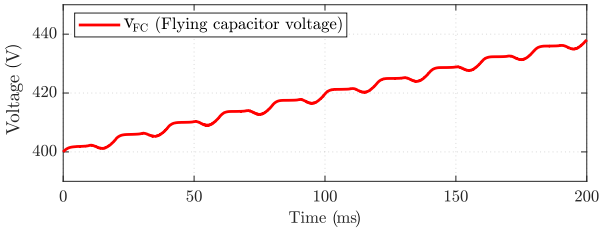

Fig. 1: Flying capacitor voltage under no-load/grid-disconnected mode (voltage fly-away condition).

The indirect MPC allows for long prediction horizons and simplifies real-time implementation since it can effectively be solved with off-the-shelf solvers. It offers better dynamic and steady-state performance and has a fixed switching frequency.

Although the previously presented control schemes achieve satisfactory system performance, some control-related issues still exist, such as the control of the flying capacitor voltage v_{FC}, as well as the deviation of the grid current from its reference. One of the main drawbacks of using the flying capacitor is that its voltage experiences a continuous increase when the load/grid is disconnected, see Fig. 1. Additionally, the flying capacitor voltage is constrained by a maximum limit of $450\,\text{V}$. Moreover, the flying capacitor must discharge during the negative cycle to a voltage less than the input dc-link voltage. When the load/grid is not present, the discharging path is open and the flying capacitor does not discharge during the negative cycle. Therefore, a continuous increase in the flying capacitor voltage is observed (termed as voltage fly-away), which is detrimental to the operation of the inverter.

One approach to address these challenges is to model the behavior of the flying capacitor in order to capture all possible dynamics of the system. Furthermore, an MPC algorithm can be adopted to handle multiple control objectives, including the control of the flying capacitor voltage under no-load/grid-disconnected condition. To this end, this paper employs a *direct* MPC scheme, as a current controller, for a single-phase grid-connected sFCI. The control objectives in grid-connected mode are the regulation of the main inductor current, grid current and the filter capacitor voltage to their references. The nonlinear discrete-time model of the converter used by the controller is designed such that it accurately predicts the plant behavior both when operating in grid-connected mode as well

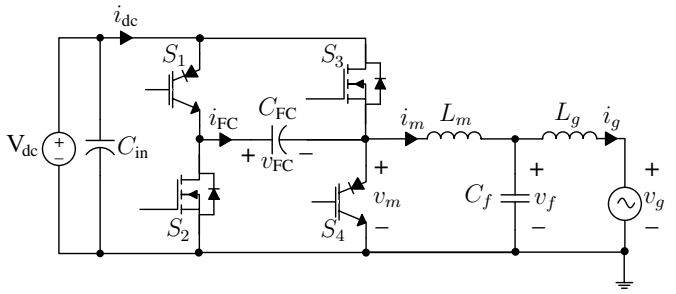

Fig. 2: Schematic diagram of a single-phase grid-connected sFCI with LCL filter.

as under no-load condition. The main contributions of this paper are: 1) the derivation of a nonlinear system model for single-phase sFCI; 2) the formulation and design of the direct MPC scheme.

II. System Modeling

Fig. 2 shows a single-phase grid-connected sFCI with an LCL filter which is based on the topology proposed in [2], [3]. The converter employs an input capacitor C_{in} for the dc link which supplies a voltage V_{dc}, and a flying capacitor C_{FC}. The LCL filter consists of a main inductor L_m and a grid-side inductor L_g, with internal resistances R_m and R_g, respectively, and the filter capacitance C_f with parasitic resistance R.

To fully describe the dynamics of the sFCI, operation of the converter is split up into six cases (see Fig. 3) unlike the three operating modes proposed in [2]. Although, the positive and negative states remain essentially the same, the zero state is further classified into four cases based on the cycle of operation (i.e., the positive or negative half-cycle with respect to the grid voltage) and the state variables.[1] Moreover, the following assumptions are introduced for the purpose of modeling:

Assumption A.1 *The switching behavior of the converter bridge is considered in the modeling stage, i.e., the flying capacitor voltage v_{FC} is defined as a system state.*

Assumption A.2 *The grid voltage $v_g(t)$ is considered as a disturbance input. It has a positive magnitude and a constant angular frequency $\omega_g > 0$.*

Assumption A.3 *The bridge voltage $v_m(t)$ is assumed to be constant during $kT_s < t < (k+1)T_s$, where T_s is the sampling interval.*

A. Continuous-Time Mathematical Model

Based on Assumption A.1, the flying capacitor voltage v_{FC} is defined as a system state. Therefore, the system states include the main inductor current, the grid current, the filter capacitor voltage and the flying capacitor voltage. Thus, the state vector is defined as

$$\boldsymbol{x} = [i_m \;\; v_f \;\; i_g \;\; v_{\text{FC}}]^\top \in \mathbb{R}^4. \tag{1}$$

[1]For details of the mathematical equations that govern the respective cases, the interested reader is referred to [4, Section 6.2].

Invoking Assumptions A.1 and A.2, Kirchhoff's current and voltage laws, and by taking into consideration the mathematical equations governing the cases of operation, a state-space representation can be written for each of the six cases shown in Fig. 3. The various state-space models can be combined into one model that precisely describes the dynamics of the sFCI when operating in different modes. To do so, similar to [7], [8], three auxiliary variables d_{aux_1}, d_{aux_2}, and d_{aux_3} are introduced and defined as

$$d_{\text{aux}_1} = \begin{cases} 1 & \text{if} \quad (h_1 \cdot b_z = 1 \text{ and } i_m > 0) \text{ or } \; h_2 \cdot b_n = 1 \\ 0 & \text{if} \quad h_1 \cdot b_p = 1 \text{ or } \; (h_1 \cdot b_z = 1 \text{ and } \; i_m < 0) \\ & \qquad \text{or } \; h_2 \cdot b_z = 1 \end{cases} \tag{2}$$

$$d_{\text{aux}_2} = \begin{cases} 1 & \text{if} \quad h_1 \cdot b_p = 1 \text{ or } \; (h_1 \cdot b_z = 1 \text{ and } \; i_m > 0) \\ 0 & \text{if} \quad h_2 = 1 \text{ or } \; (h_1 \cdot b_z = 1 \text{ and } \; i_m < 0) \end{cases} \tag{3}$$

$$d_{\text{aux}_3} = \begin{cases} 1 & \text{if} \quad v_{\text{FC}} < V_{\text{dc}} \text{ and } \; i_m < 0 \\ 0 & \qquad \text{otherwise} \end{cases} \tag{4}$$

Here, the binary variables h_1 and h_2 denote the positive and negative half-cycles of operation, respectively. The binary variables b_p, b_n and b_z represent the positive (P), negative (N) and zero (O) states of operation, respectively.[2]

Taking all the above into account, the complete model of the system is written as

$$\frac{\mathrm{d}\boldsymbol{x}(t)}{\mathrm{d}t} = \mathbf{F}\boldsymbol{x}(t) + \mathbf{G}V_{\text{dc}}(t) + \mathbf{T}_1 v_g(t) + \mathbf{T}_2 i_{\text{dc}}(t) \tag{5a}$$

$$\boldsymbol{y}(t) = \mathbf{C}\boldsymbol{x}(t) \tag{5b}$$

where the system matrices of the complete model are

$$\mathbf{F} = \begin{bmatrix} -\frac{R+R_m}{L_m} & -\frac{1}{L_m} & \frac{R}{L_m} & -\frac{d_{\text{aux}_1}}{L_m} \\ \frac{1}{C_f} & 0 & -\frac{1}{C_f} & 0 \\ \frac{R}{L_g} & \frac{1}{L_g} & -\frac{R+R_g}{L_g} & 0 \\ \frac{d_{\text{aux}_1}}{C_{\text{FC}}} & 0 & 0 & 0 \end{bmatrix},$$

$$\mathbf{G} = \begin{bmatrix} \frac{d_{\text{aux}_2}}{L_m} \\ 0 \\ 0 \\ 0 \end{bmatrix}, \mathbf{T}_1 = \begin{bmatrix} 0 \\ 0 \\ -\frac{1}{L_g} \\ 0 \end{bmatrix}, \mathbf{T}_2 = \begin{bmatrix} 0 \\ 0 \\ 0 \\ \frac{d_{\text{aux}_3}}{C_{\text{FC}}} \end{bmatrix}, \mathbf{C} = \mathbf{I}_4. \tag{6}$$

Fig. 4 depicts the sFCI represented as a continuous-time automaton. As can be seen, transitions from one case of operation to another are specified by the auxiliary variables, along with the state variables of the converter and its states of operation.

B. Discrete-Time Mathematical Model

Based on Assumptions A.2 and A.3, the continuous-time model (5) is discretized using exact discretization. This yields the discrete-time model

$$\boldsymbol{x}(k+1) = \mathbf{A}\boldsymbol{x}(k) + \mathbf{B}V_{\text{dc}}(k) + \mathbf{E}_1 v_g(k) + \mathbf{E}_2 i_{\text{dc}}(k) \tag{7a}$$

$$\boldsymbol{y}(k) = \mathbf{C}\boldsymbol{x}(k+1) \tag{7b}$$

[2]For a detailed description of the states of operation, see [4, Section 3.1].

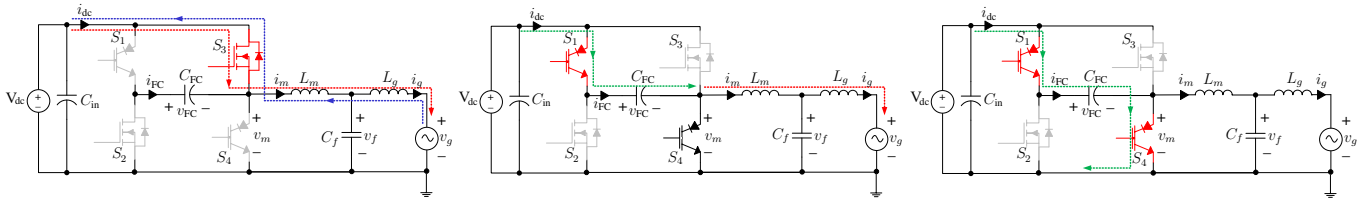

(a) Case 1 : Positive state. (b) Case 2 : Zero-state while $i_m > 0$. (c) Case 3 : Zero-state while $i_m < 0$.

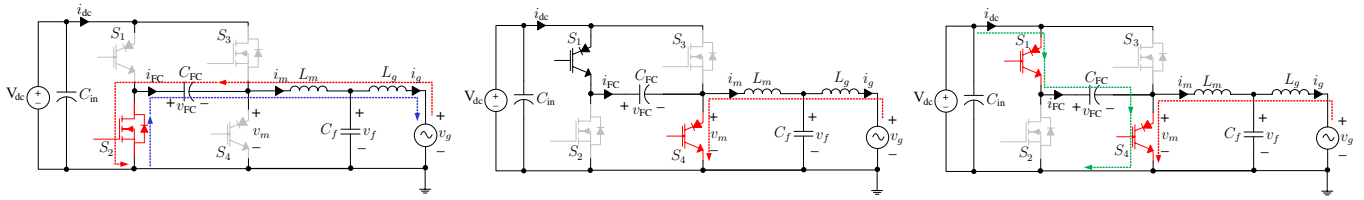

(d) Case 4 : Negative state. (e) Case 5 : Zero-state while $V_{\text{dc}} < v_{\text{FC}}$. (f) Case 6 : Zero-state while $V_{\text{dc}} > v_{\text{FC}}$.

Fig. 3: Schematic overview of the operation cases with respective current flows denoted as: active current (red dotted line), reactive current (blue dotted line), and flying capacitor charging current (green dotted line).

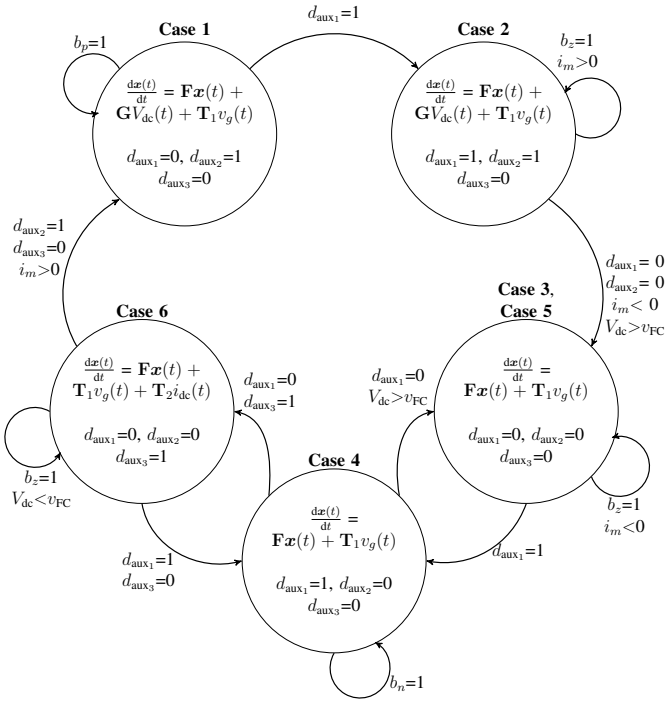

Fig. 4: sFCI presented as a continuous-time automaton.

where $k \in \mathbb{N}$ is the discrete-time index, T_s is the sampling interval, and the discrete-time system matrices are

$$\mathbf{A} = e^{\mathbf{F}T_s}, \quad \mathbf{B} = \left(\int_0^{T_s} e^{\mathbf{F}\tau} \cdot e^{\mathrm{j}\omega_g \tau} d\tau \right) \mathbf{G},$$
$$\mathbf{E}_h = \left(\int_0^{T_s} e^{\mathbf{F}\tau} \cdot e^{\mathrm{j}\omega_g \tau} d\tau \right) \mathbf{T}_h \quad \text{where } h \in \{1, 2\}. \tag{8}$$

III. Direct Model Predictive Control

Direct MPC has recently received a lot of attention, see e.g., [9]–[14]. It does not employ a modulator as the switching signals are generated directly from the controller. Its advantages include simplicity of the concept, faster dynamics and flexibility in terms of the control target realization. In the past decade, research on direct MPC has spread across various fields, e.g., renewable energy systems, multilevel converters, and electrical drives [13].

A. Control Objectives

For the sFCI, there are multiple control objectives. Firstly, the grid current i_g should accurately track its reference $i_{g,\text{ref}}$. Secondly, the main inductor current i_m and the filter capacitor voltage v_f should be regulated along their reference trajectories $i_{m,\text{ref}}$ and $v_{f,\text{ref}}$. Additionally, the voltage of the flying capacitor must be controlled during no-load operation. Moreover, the switching losses should be relatively low, which can be achieved indirectly by controlling the switching frequency. Finally, during transients, the above-mentioned controlled variables should quickly reach their desired values and with as little overshoot as possible.

In order to achieve the above mentioned objectives the control of the sFCI is split up into two schemes, i.e.,

I. when the sFCI has no load, i.e., grid-disconnected condition,
II. when the sFCI is on load, i.e., grid connected and/or steady-state operating conditions exist.

B. Control Procedure

Fig. 5 illustrates the block diagram of the proposed controller for the single-phase sFCI. The desired system performance can be achieved by directly manipulating the inverter switches, without using a modulator. The switch position is modeled by $u \in \{-1, 0, 1\}$ where 1 corresponds to the case where switch S_3 is on, 0 when S_1 and S_4 are on, and -1 when S_2 is on, see Fig. 2. The direct MPC algorithm first computes the evolution of the plant over the prediction horizon (i.e., the trajectories of the variables of concern) based on the measurements of the grid current, main inductor current, filter capacitor voltage, flying capacitor voltage, and grid voltage. Following this, the optimal control action (i.e., the switching signal) is chosen by minimizing a performance criterion in real

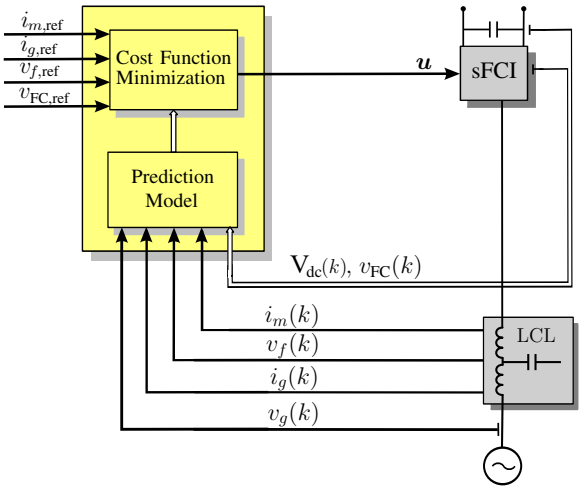

Fig. 5: Block diagram of the direct MPC for a single-phase sFCI based on the automaton approach.

time. To mitigate the voltage fly-away condition of the flying capacitor, the controller works in the Scheme-I. Whenever the system is grid connected, the controller changes to Scheme-II where the flying capacitor voltage does not require further regulation.

***Control Scheme-I**:* As highlighted previously, constraining the flying capacitor voltage below $450\,\text{V}$ is crucial for the operation of the sFCI. Control Scheme-I primarily aims at maintaining the flying capacitor voltage near a reference value. This is possible if a discharging path is available or if the flying capacitor is not charged continuously during the positive cycle.

In direct MPC, the transitions between the upper and lower rails are forbidden due to switching constraints. For control Scheme-I, the switching constraints are relaxed and switching from 1 to -1, and vice versa, in one time step is allowed. This allows the controller to generate a switching pattern wherein the flying capacitor does not undergo continuous charging and mitigation of the voltage fly-away condition is possible.

***Control Scheme-II**:* During this scheme, the switching constraints are reinstated, i.e., direct transitions between -1 and 1 are forbidden. The control objectives relate to the grid current control with regulation of the main inductor current and filter capacitor voltage, while the voltage of the flying capacitor is indirectly maintained within allowable limits. Essentially, the system model simplifies to the LCL filter/grid system and the controller tackles the converter as a conventional three-level inverter.

C. Optimization Problem

The discrete-time model (7) is used to predict the future trajectory of the system output $\boldsymbol{y}$. At time-step k, the cost function that penalizes the error of the output variables over the finite prediction horizon of N_p time steps is formulated as

$$J(k) = \sum_{\ell=k}^{k+N_p-1} \|\boldsymbol{y}_{\text{ref}}(\ell+1) - \boldsymbol{y}(\ell+1)\|_{\boldsymbol{Q}}^2 + \lambda_u \|\Delta u(\ell)\|_2^2 \,. \tag{9}$$

TABLE I: System parameters and controller data.

Parameter	Symbol	Value
Nominal power	P_n	$1.7\,\text{kW}$
Converter-side inductance	L_m	$400\,\mu\text{H}$
Converter-side resistance	R_m	$70\,\text{m}\Omega$
Grid-side inductance	L_g	$56\,\mu\text{H}$
Grid-side resistance	R_g	$30\,\text{m}\Omega$
Filter capacitance	C_f	$5\,\mu\text{F}$
ESR of filter capacitor	R	$7.4\,\text{m}\Omega$
Flying capacitor	C_{FC}	$680\,\mu\text{F}$
DC-link voltage	V_{dc}	$400\,\text{V}$
Nominal grid voltage	v_g	$230\,\text{V(rms)}$
Grid inductance	L_{grid}	$0.01\,\text{mH}$
Grid resistance	R_{grid}	$0.1\,\Omega$
Resonance frequency	f_r	$10.155\,\text{kHz}$
Sampling time	T_s	$4\,\mu\text{s}$
Controller step time	T_{ctl}	$4\,\mu\text{s}$

In (9), $\boldsymbol{y}_{\text{ref}} \in \mathbb{R}^4$ encompasses the reference values of the controlled variables (main inductor current, filter capacitor voltage, grid current, and flying capacitor voltage), i.e.,

$$\boldsymbol{y}_{\text{ref}} = [i_{m,\text{ref}} \;\; v_{f,\text{ref}} \;\; i_{g,\text{ref}} \;\; v_{\text{FC,ref}}]^\top \,. \tag{10}$$

The first term of the cost function implements the objective of reference tracking with $\boldsymbol{Q} \in \mathbb{R}^{4\times4}$ as the weighting factor matrix. Matrix $\boldsymbol{Q}$ is positive semidefinite and its diagonal entries are chosen in a way that the tracking accuracy among the four controlled variables is prioritized. The second term implements the minimization of switching effort $\Delta u(\ell) = u(\ell) - u(\ell-1)$, where penalization is carried out using a nonnegative weighting factor λ_u.

With Scheme-I, priority is given to the flying capacitor voltage control by penalizing the corresponding error more heavily, while λ_u is set to zero. On the other hand, Scheme-II has three control objectives, i.e., the control of the three states i_g, i_m and v_f. In this control scheme, $\boldsymbol{Q}$ is chosen such that it highly penalizes the grid current error as compared to the errors in main inductor current and filter capacitor voltage, while the weighting factor related to flying capacitor voltage is set to zero.

Finally, the optimal sequence of control actions

$$\boldsymbol{U}^*(k) = [u^*(k) \;\; u^*(k+1) \;\; \ldots \;\; u^*(k+N_p-1)]^\top$$

is computed by minimizing (9) subject to the system models and the switching constraint for Scheme-II. Only the first element $u^*(k)$ of this optimal sequence is utilized, whereas the rest are discarded. At the next time step $k+1$, the complete procedure is repeated based on updated measurements over a one-step shifted horizon, according to the receding horizon policy [13].

IV. Performance Evaluation of Direct MPC

In this section, simulation results are presented to demonstrate the performance of the proposed direct MPC scheme. The system under consideration is a single-phase sFCI rated for $1.7\,\text{kW}$. Table I contains the system and controller parameters. The weighting factor matrices $\boldsymbol{Q}_1 = \text{diag}(10, 10, 1, 40)$ and $\boldsymbol{Q}_2 = \text{diag}(20, 90, 1, 0)$ correspond to control Scheme-I

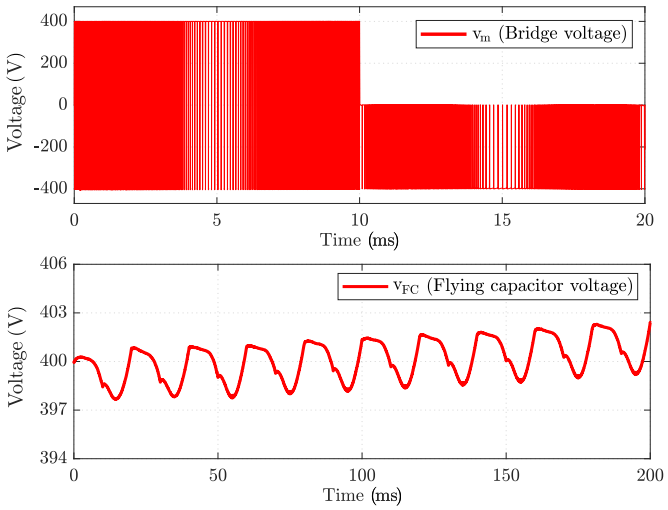

Fig. 6: Performance of the single-phase sFCI under control Scheme-I, while it is disconnected from the grid.

and -II, respectively. The control effort weighting factor is set to $\lambda_u = 0.2$. Finally, a three-step prediction horizon ($N_p = 3$) is implemented.

A. System Performance With Control Scheme-I

Control Scheme-I is used when the sFCI is disconnected from the grid. The response of the system during this scheme is shown in the Fig. 6. As an observation, the converter bridge voltage during the positive half-cycle (with respect to the grid voltage) resembles a two-level inverter output. This is due to the fact that the switching constraint has been relaxed and the converter is allowed to directly switch between the upper and lower rails, i.e., 1 and -1.

During the grid-disconnected mode, the controller is tasked to control the voltage of the flying capacitor with the weighting factor matrix $\boldsymbol{Q}_1$. This imposes a large cost on the flying capacitor voltage error and therefore the controller commands the converter to switch between the positive and negative states to prevent continuous charging of the flying capacitor C_{FC} during the intermediate zero states. Fig. 6 shows the voltage v_{FC} for 10 cycles of operation. Compared to the conventional control schemes (see Fig. 1) where the voltage increases by 40 V within the same time internal, the system operated with control Scheme-I exhibits a voltage rise of merely 3 V. Therefore, the voltage fly-away condition can be effectively mitigated without the use of any additional components, and the voltage of the flying capacitor can be maintained within permitted limits.

B. System Performance With Control Scheme-II

When the sFCI is grid connected the controller operation changes from Scheme-I to Scheme-II. As indicated previously, the switching constraints are activated again, thus the converter is not allowed to directly switch between the two extreme states. The controller ensures reference tracking of the three variables of concern i_m, v_f, and i_g with weighting factor

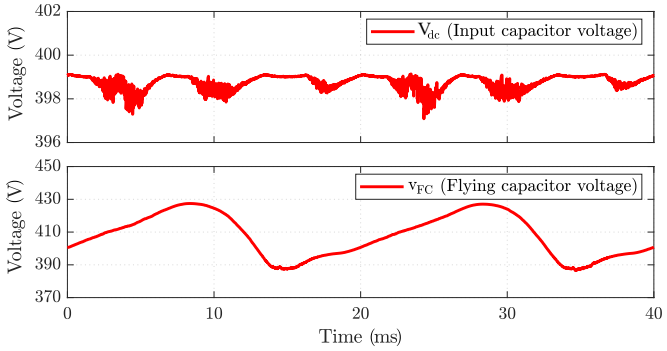

(a) Voltage waveforms for the input dc link and flying capacitor.

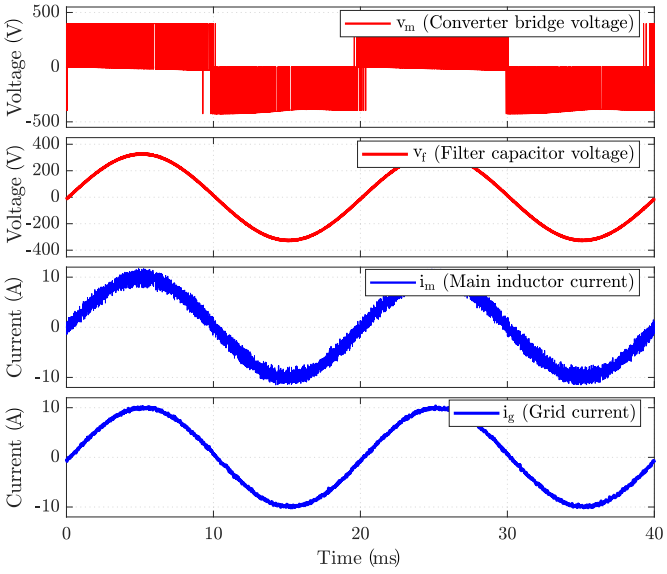

(b) Converter bridge voltage and states of the LCL filter

Fig. 7: Steady-state performance of the grid-connected single-phase sFCI during control Scheme-II with a prediction horizon $N_p = 3$.

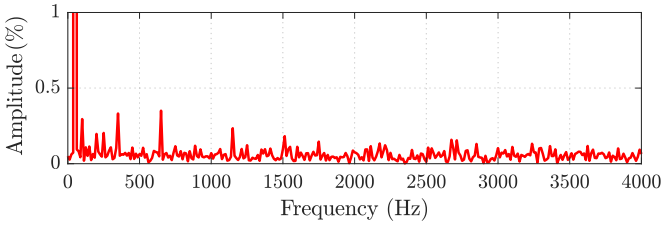

Fig. 8: Harmonic spectrum of grid current. The THD is 2.4%.

matrix $\boldsymbol{Q}_2$. Unlike Scheme-I, the flying capacitor voltage does not require direct regulation.

For a real power reference of 1.6 kW, the grid current reference (peak) $i_{g,\text{ref}}$ is set to 10 A. The steady-state performance of the single-phase sFCI is shown in Figs. 7(a) and 7(b). The flying capacitor voltage has a constant ripple and is maintained below the allowable limit of 450 V, see Fig. 7(a). The grid current is sinusoidal with total harmonic distortion (THD) of 2.4% (see Fig. 8 for the harmonic spectrum). Unlike the state-feedback control of sFCI in [4], [5], where the grid current deviates from the sinusoidal behavior due to an uneven bump around zero crossing, the proposed direct MPC

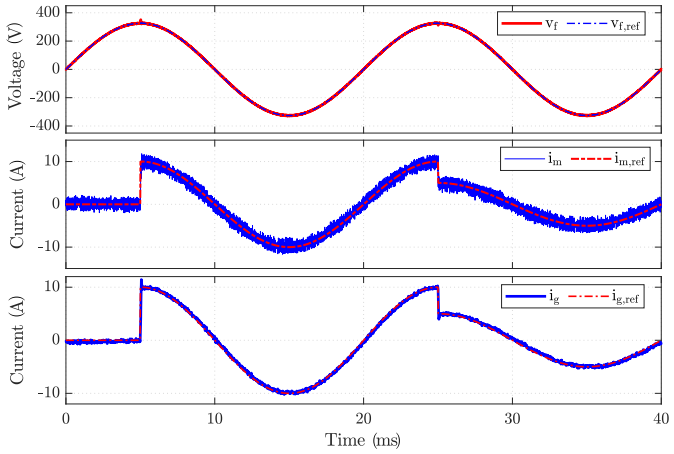

Fig. 9: Dynamic performance of the grid-connected single-phase sFCI during control Scheme-II with a prediction horizon $N_p = 3$.

algorithm achieves an improved current response. Moreover, the controller operates the converter at an average switching frequency of 29 kHz.

The dynamic performance of the direct MPC is shown in Figs. 9 and 10. At 5 ms the reference current is set to 10 A and at 25 ms it is decreased to 5 A. In Fig. 9, the three states of the LCL filter are compared with their respective references. As can be seen, the presented direct MPC has excellent transient response with minimal overshoot. Figs. 10(a) and 10(b) show the tracking performance of the grid current when the current steps are initiated. It can be observed that, the controller follows the reference trajectories with negligible overshoot and very short settling time.

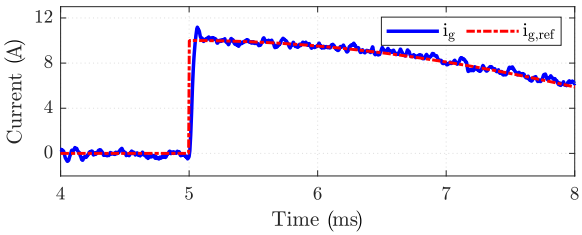

(a) The grid current reference is set to 10 A at 5 ms.

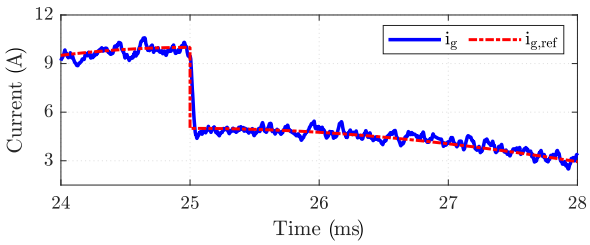

(b) The grid current reference is decreased to 5 A at 25 ms.

Fig. 10: Reference tracking of the grid currents.

V. Conclusion

In this paper, a direct model predictive control (MPC) approach based on enumeration is presented for a grid-connected single-phase sFCI. To mitigate the voltage fly-away condition, a discrete-time nonlinear switched model of the converter is derived that accurately captures all modes of operation. With this model at hand, the proposed control technique manages to control the system under both grid-disconnected and grid-connected mode. As shown, Scheme-I of the discussed hybrid control algorithm successfully controls the voltage of the flying capacitor during off-grid conditions. Moreover, owing to the introduced control Scheme-II effective output reference tracking is achieved. Based on the presented results, it can be concluded that the presented MPC scheme has a better dynamic performance compared to the linear state-feedback controller [5], with shorter settling times and superior reference tracking during steady-state conditions.

References

[1] S. Kouro, J. I. Leon, D. Vinnikov, and L. G. Franquelo, "Grid-connected photovoltaic systems: An overview of recent research and emerging PV converter technology," *IEEE Ind. Electron. Mag.*, vol. 9, no. 1, pp. 47–61, Mar. 2015.

[2] Y. P. Siwakoti and F. Blaabjerg, "A novel flying capacitor transformerless inverter for single-phase grid connected solar photovoltaic system," in *Proc. IEEE Int. Symp. on Power Electron. for Distrib. Gen. Sys.*, Vancouver, BC, Canada, Jun. 2016, pp. 1–6.

[3] Y. P. Siwakoti and F. Blaabjerg, "Common-ground-type transformerless inverters for single-phase solar photovoltaic systems," *IEEE Trans. Ind. Electron.*, vol. 65, no. 3, pp. 2100–2111, Mar. 2018.

[4] M. A. W. Begh, "Closed Loop Current Control of a Grid Connected Transformerless Flying Capacitor Inverter," MSc thesis, Technical University of Munich, Munich, Germany, Nov. 2018.

[5] M. A. W. Begh, E. Liegmann, A. Mahajana, A. Palanisamy, Y. Siwakoti, P. Karamanakos, M. Abdelrahem, and R. Kennel, "Design of state-feedback controller for a single-phase grid-connected Siwakoti-H inverter with LCL filter," in *Proc. Int. Exhib. and Conf. for Power Electron., Intell. Motion, Renew. Energy and Energy Manag.*, Nuremberg, Germany, May 2019, pp. 1587–1594.

[6] M. A. W. Begh, E. Liegmann, P. Karamanakos, A. Mahajan, Y. Siwakoti, and R. Kennel, "Indirect model predictive control of a three-phase grid-connected Siwakoti-H inverter," in *Proc. IEEE Ind. Electron. Conf.*, Lisbon, Portugal, Oct. 2019, pp. 411–416.

[7] P. Karamanakos, T. Geyer, and S. Manias, "Direct voltage control of dc-dc boost converters using enumeration-based model predictive control," *IEEE Trans. Power Electron.*, vol. 29, no. 2, pp. 968–978, Feb. 2014.

[8] A. Ayad, P. Karamanakos, and R. Kennel, "Direct model predictive current control strategy of quasi-Z-source inverters," *IEEE Trans. Power Electron.*, vol. 32, no. 7, pp. 5786–5801, Jul. 2017.

[9] S. Kouro, P. Cortés, R. Vargas, U. Ammann, and J. Rodríguez, "Model predictive control—a simple and powerful method to control power converters," *IEEE Trans. Ind. Electron.*, vol. 56, no. 6, pp. 1826–1838, Jun. 2009.

[10] J. Rodríguez, M. P. Kazmierkowski, J. R. Espinoza, P. Zanchetta, H. Abu-Rub, H. A. Young, and C. A. Rojas, "State of the art of finite control set model predictive control in power electronics," *IEEE Trans. Ind. Informat.*, vol. 9, no. 2, pp. 1003–1016, May 2013.

[11] P. Karamanakos, T. Geyer, N. Oikonomou, F. D. Kieferndorf, and S. Manias, "Direct model predictive control: A review of strategies that achieve long prediction intervals for power electronics," *IEEE Ind. Electron. Mag.*, vol. 8, no. 1, pp. 32–43, Mar. 2014.

[12] S. Vazquez, J. Rodriguez, M. Rivera, L. G. Franquelo, and M. Norambuena, "Model predictive control for power converters and drives: Advances and trends," *IEEE Trans. Ind. Electron.*, vol. 64, no. 2, pp. 935–947, Feb. 2017.

[13] T. Geyer, *Model predictive control of high power converters and industrial drives*. John Wiley & Sons, Sep. 2016.

[14] P. Karamanakos and T. Geyer, "Guidelines for the design of finite control set model predictive controllers," *IEEE Trans. Power Electron.*, vol. 35, no. 7, pp. 7434–7450, Jul. 2020.